Philosophical Magazine, 11 December 2003
Vol. 83, No. 35, 3959–3976

Taylor & Francis
Taylor & Francis Group

Experimental and computational creep characterization of Al–Mg solid-solution alloy through instrumented indentation

Hidenari Takagi

Department of Mechanical Engineering, College of Engineering, Nihon University, Tamuramachi, Koriyama, Fukushima 963-8642, Japan

Ming Dao†

Department of Materials Science and Engineering, Massachusetts Institute of Technology, Cambridge, Massachusetts 02139, USA

Masami Fujiwara‡

Department of Applied Physics, College of Engineering, Nihon University, Tamuramachi, Koriyama, Fukushima 963-8642, Japan

and Masahisa Otsuka

Department of Materials Science and Engineering, Faculty of Engineering, Shibaura Institute of Technology, Tokyo 108-8548, Japan

[*Received 30 May 2003 and accepted in revised form 20 August 2003*]

Abstract

Carefully designed indentation creep experiments and detailed finite-element computations were carried out in order to establish a robust and systematic method to extract creep properties accurately during indentation creep tests. Samples made from an Al–5.3 mol% Mg solid-solution alloy were tested at temperatures ranging from 573 to 773 K. Finite-element simulations confirmed that, for a power-law creep material, the indentation creep strain field is indeed self-similar in a constant-load indentation creep test, except during short transient periods at the initial loading stage and when there is a deformation mechanism change. Self-similar indentation creep leads to a constitutive equation from which the power-law creep exponent n, the activation energy Q_c for creep, the back or internal stress and so on can be evaluated robustly. The creep stress exponent n was found to change distinctively from 4.8 to 3.2 below a critical stress level, while this critical stress decreases rapidly with increasing temperature. The activation energy for creep in the stress range of $n = 3.2$ was evaluated to be 123 kJ mol^{-1}, close to the activation energy for mutual diffusion of this alloy, 130 kJ mol^{-1}. Experimental results suggest that, within the $n = 3.2$ regime, the creep is rate controlled by viscous glide of dislocations which drag solute atmosphere and the back or internal stress is proportional to the average applied stress. These results are in good agreement with those obtained from conventional uniaxial

†Author for correspondence. Email: mingdao@mit.edu.
‡Author for correspondence. Email: fujiwara@ge.ce.nihon-u.ac.jp.

Philosophical Magazine ISSN 1478–6435 print/ISSN 1478–6443 online
http://www.tandf.co.uk/journals
DOI: 10.1080/14786430310001616045

creep tests in the dislocation creep regime. It is thus confirmed that indentation creep tests of Al–5.3 mol% Mg solid-solution alloy at temperatures ranging from 573 to 773 K can be effectively used to extract material parameters equivalent to those obtained from conventional uniaxial creep tests in the dislocation creep regime.

§ 1. Introduction

With new materials being invented daily in research and development, they are often available only in minute quantities or as small volume samples or structures. It is very important to establish a robust and convenient mechanical testing method that can accurately extract mechanical properties at both ambient and high temperatures from these small-volume materials. Instrumented indentation has been widely used to extract elastic and elastoplastic mechanical properties at low temperatures and to estimate creep properties at high temperatures.

Considerable efforts and significant progresses have been made in extracting ambient temperature elastic and elastoplastic properties (Tabor 1951, Oliver and Pharr 1992, Field and Swain 1995, Gerberich *et al.* 1996, Dao *et al.* 2001). Many pioneering studies have been conducted on indentation creep as well. One of the earliest studies regarding indentation hardness versus loading time was carried out by Tabor and his co-workers (Mulhearn and Tabor 1960, Atkins *et al.* 1966). Li *et al.* (1991) tried to analyse all deformation mechanisms which may contribute to indentation creep. Sargent and Ashby (1992) demonstrated that the hot-hardness test provides information concerning the time-dependent flow, or creep, of the material beneath the self-similar indenter. Prakash (1996) proposed a conceptual model for analysing self-similar indentation creep data in terms of the back or internal stresses resulting from the interaction of mobile dislocations with microstructural inhomogeneities. Lucas and Oliver (1999) investigated the dependence of hardness on indentation strain rate and temperature and discussed steady-state deformation behaviour in nanoindentation. Mackerle (2001) summarized a bibliography of recent papers on computer simulations for indentation problems. Assuming self-similarity under a constant load, Fujiwara and Otsuka (1999, 2001) derived a set of constitutive equations for self-similar indentation creep and performed experiments on pure Sn and Sn-based eutectic alloy. Excluding elasticity effects, Cheng and Cheng (2001) proposed several scaling relationships using dimensional analysis. Creep studies using a cylindrical indenter were also carried out (Li 2002), and those experiments were often called 'impression tests'.

However, an indentation stress or strain field is a highly non-uniform field that depends on the prior plastic deformation history, and an indentation creep test often involves transient periods (including the initial loading period as well as the transition period when there is a deformation mechanism change at different applied stress levels). Therefore, a number of important questions remain that require further investigation:

(i) whether or not the initial transient response, which is apparently not self-similar, will result in the loss of self-similarity throughout the entire indentation creep process;
(ii) if the self-similar indentation creep is eventually reached, how long it takes to reach that stage;

(iii) whether or not one can accurately extract creep properties during indentation creep tests.

Considering the complications related to these issues, they can only be properly resolved via carefully designed experiments together with corresponding detailed numerical analyses.

In the present study, constant-load indentation creep tests of an Al–5.3 mol% Mg solid-solution alloy are performed at temperatures ranging from 573 K to 773 K (from $0.63T_m$ to $0.85T_m$, where T_m is the absolute melting temperature), computational and experimental verifications are carried out to examine the self-similarity assumption during constant-load indentation creep tests, and analytical equations are given for systematically extracting the creep exponent n, the creep activation energy Q_c and the critical stress σ_c for breakaway of dislocations from their solute atmosphere. High-temperature deformation mechanisms of Al–Mg solid-solution alloy are discussed in connection with all our experimental results. Comparison with available experimental results in the literature is also given.

§ 2. Experimental, theoretical and computational considerations

2.1. *Experimental procedures*

Ingots of Al–5.3 mol% Mg alloy were homogenized by keeping in Ar gas for 86.4 ks at 773 K ($0.85T_m$). They were cut into approximately 10 mm × 5 mm × 5 mm pieces with a metal saw and carefully shaped into parallelepipeds using special jigs and emery papers. All specimens were subjected to annealing in Ar gas for 3.6 ks at 773 K. After that, they were electropolished and acid cleaned to remove the surface layer of up to about 40 μm in thickness and immediately placed in the testing machine in order to minimize atmospheric tarnish. The chemical composition of the specimens is shown in table 1.

Several specimens were treated in a suitable etchant with a current density of 400 kA m^{-2} for 90 s at 273 K and observed under a metallurgical microscope. The etching solution consists of 10 ml of perchloric acid, 20 ml of ethylene glycol and 400 ml of ethanol. The microstructure images were processed with grain-size analysis software. No significant changes were observed in grain size before and after indentation creep tests, and the average grain diameter was around 410 μm. The grain size did not change even in the region just below the indentation contact impression. Therefore, the grain size is treated as constant at a given temperature.

Figure 1 (*a*) schematically shows the instrumented microindenter used in this study. This indentation tester was built in collaboration with ULVAC-RIKO in Japan (Fujiwara and Otsuka 1999). The quartz indenter column moves downwards from its equilibrium position by an electromagnetic force, and the diamond indenter tip is then pressed perpendicularly into a 10 mm × 5 mm surface area of the heated specimen in an Ar gas atmosphere. The indentation depth can be obtained by

Table 1. Chemical composition of tested materials.

	Analysed composition (mol%)				
Test material	Mg	Si	Fe	Cu	Al
Al–5.3 mol% Mg alloy	5.3	0.004	0.004	0.0002	Balance

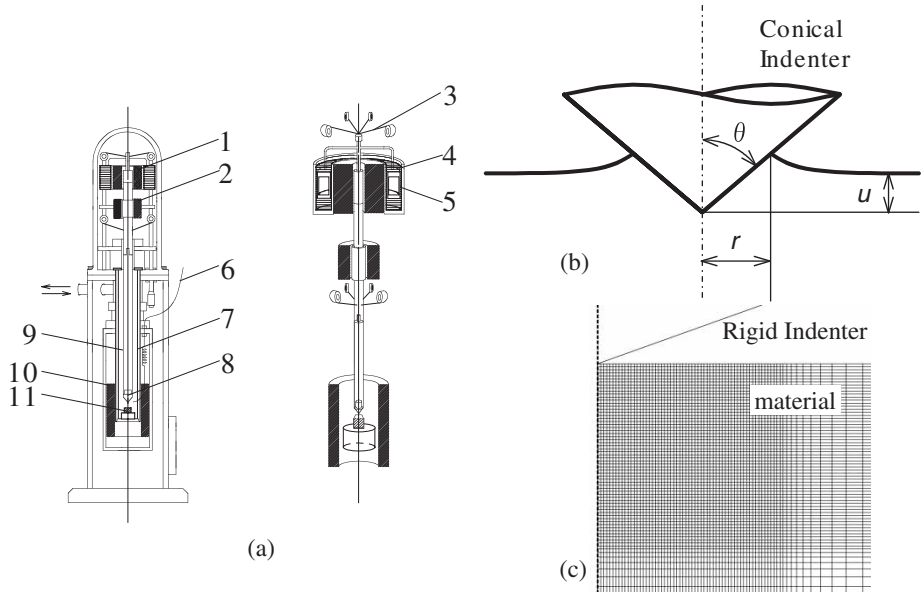

Figure 1. (*a*) Schematic diagrams of the microindenter (maximum load, 4.9 N; maximum temperature, 1073 K; displacement resolution, 0.05×10^{-6} m): 1, solenoid; 2, LVDT; 3, lines; 4, oil bath; 5, float; 6, thermocouple; 7, quartz tube; 8, indenter tip; 9, quartz indenter column; 10, heater; 11, specimen. (*b*) Schematic drawing of the conical indenter penetrating the test material. (*c*) Mesh design for the finite-element calculations.

measuring the displacement of the indenter column with a linear variable-differential transformer (LVDT). Since the LVDT is placed more than 30 cm away from the heater, the thermal drift error is carefully controlled to be negligible compared with the micron-scale indenter displacement. During an indentation creep test, data for load and indenter displacement are recorded versus indentation time. It is often seen that indentation creep curves vary a little in shape as well as magnitude at different sampling points even on the same specimen. Similar dispersions can also be observed during hardness tests. Nevertheless, after training in operating the microindenter for 1 week, indentation creep curves are repeatable in three out of seven trials according to our experience.

Indentation creep tests for Al–5.3 mol% Mg alloy were carried out under such conditions that dynamic recrystallization does not occur. The test conditions applied are as follows: test temperatures, 573–773 K ($0.63T_m$–$0.85T_m$); indentation load, 0.39 N; total indentation time, 1200 s.

The indenter tip is conical in shape up to a height of 120 μm (the included half-apex-angle $\theta = 68^\circ$). The temperature variation during indentation creep test was within ±1 K. The applied load could reach the desired value within less than 0.1 s.

2.2. *Constitutive equation of indentation creep*

When a sharp indenter is pressed into the surface of a heated specimen, it penetrates with the rate-dependent and temperature-dependent yielding and creeping of the indented sample. The time-dependent flow, or creep, of the material below the indenter is called indentation creep (Li *et al.* 1991, Sargent and

Ashby 1992, Prakash 1996). Using a self-similar sharp indenter (e.g. cone or pyramid), it is often assumed that the plastic region just below the indenter extends while maintaining its geometrical self-similarity as indentation creep proceeds; that is the contours of plastic strain change only in scale, and not in shape (Hill 1983). Assuming that the material's creep behaviour obeys the well-known creep law for uniaxial steady-state creep (Mukherjee *et al.* 1969, Cadek 1988) given by

$$\dot{\varepsilon}^{\mathrm{c}} = A_1\left(\frac{\sigma}{E}\right)^n\left(\frac{b}{d}\right)^q \exp\left(-\frac{Q_{\mathrm{c}}}{RT}\right), \tag{1 a}$$

a constitutive equation was given for the self-similar indentation creep (Fujiwara and Otsuka 1999):

$$\dot{u} = A_2 u\left(\frac{F}{Eu^2}\right)^n\left(\frac{b}{d}\right)^q \exp\left(-\frac{Q_{\mathrm{c}}}{RT}\right), \tag{1 b}$$

where $\dot{\varepsilon}^{\mathrm{c}}$ is the effective creep strain rate of the indented material, $\dot{u}$ is the indenter velocity, A_1 and A_2 are constants with the dimension of the reciprocal of time, σ is the von Mises flow stress, u is the indenter displacement, F is the indentation load, E is Young's modulus at the test temperature, b is the magnitude of the Burgers vector, d is the grain size, R is the gas constant and T is the test temperature. The power-law creep exponent n, the grain-size exponent q and the activation energy Q_{c} for creep are constants that are uniquely determined by the predominant rate-controlling process of creep deformation. Many uniaxial creep tests showed that dislocation creep rate is only slightly influenced by grain size; therefore $q=0$ is usually set in equations (1 *a*) and (1 *b*).

When T and d are constant during indentation creep under a given F, the stress exponent n in equation (1 *b*) is given by

$$n = \frac{1}{2}\left(1 - \frac{\partial(\ln \dot{u})}{\partial(\ln u)}\right)_{T,d}. \tag{2}$$

Setting $K = \dot{u}(Eu^2/F)^n/u$, equation (1 *b*) is rewritten as

$$K = A_2\left(\frac{b}{d}\right)^q \exp\left(-\frac{Q_{\mathrm{c}}}{RT}\right). \tag{3}$$

The K parameter has the dimension of the reciprocal of time. When d is kept constant regardless of the temperature employed, the activation energy Q_{c} for creep is obtained by

$$Q_{\mathrm{c}} = -R\left(\frac{\partial(\ln K)}{\partial(1/T)}\right)_d. \tag{4}$$

Equations (2)–(4) were proposed by Fujiwara and Otsuka (1999, 2001) and applied to study pure Sn and Sn-based eutectic alloy.

The load on the indenter is carried by a projected contact area A of an impression. The contact area is proportional to u^2 for a self-similar indentation, that is $A \propto u^2$. For equilibrium, the indentation pressure p is expressed by $p = F/A$, which is called the Meyer hardness. When the friction between the indenter and the material being tested is negligibly small, the representative flow stress $\overline{\sigma}$ in the

plastic region below the indenter can be approximately written as (Tabor 1951, Johnson 1970, Bolshakov and Pharr 1998)

$$\overline{\sigma} \approx \frac{p}{3} \propto \frac{F}{u^2}. \tag{5}$$

Here $\overline{\sigma}$ is a measurement of the average equivalent (von Mises) stress in the plastic zone. When the plastic zone extends in such a way that its configuration remains geometrically self-similar as indentation creep proceeds, the indentation strain rate $\dot{\varepsilon}_{\text{ind}}$ is defined as (Atkins *et al.* 1966, Mayo and Nix 1988, Asif and Pethica 1997)

$$\dot{\varepsilon}_{\text{ind}} = \frac{\dot{u}}{u} = \frac{\mathrm{d}(\ln u)}{\mathrm{d}t}. \tag{6}$$

Substituting equations (5) and (6) into equation (1 *b*) gives

$$\dot{\varepsilon}_{\text{ind}} = A_3 \left(\frac{\overline{\sigma}}{E}\right)^n \left(\frac{b}{d}\right)^q \exp\left(-\frac{Q_{\text{c}}}{RT}\right). \tag{7}$$

The above equation is in the same form as equation (1 *a*) in appearance. Here A_3 is a constant that has the dimension of the reciprocal of time. From equation (7), the stress exponent n for creep can now be obtained by

$$n = \left(\frac{\partial(\ln \dot{\varepsilon}_{\text{ind}})}{\partial[\ln(\overline{\sigma}/E)]}\right)_{T,d}. \tag{8}$$

This expression shows that the n value measures the stress sensitivity of the indentation strain rate $\dot{\varepsilon}_{\text{ind}}$.

2.3. *Computational model set-up*

To compute the indentation creep behaviour, the uniaxial formulation of creep in equation (1 *a*) has to be extended to the spatial tensor formulation. A brief description is given below.

The total strain tensor $\boldsymbol{\varepsilon}$ is decomposed into the elastic part $\boldsymbol{\varepsilon}^{\text{e}}$ and creep (plastic) part $\boldsymbol{\varepsilon}^{\text{c}}$:

$$\boldsymbol{\varepsilon} = \boldsymbol{\varepsilon}^{\text{e}} + \boldsymbol{\varepsilon}^{\text{c}}. \tag{9}$$

Replacing the uniaxial stress and uniaxial strain measures to be effective values in equation (1), that is

$$\sigma = \left(\frac{3}{2}\right)^{1/2} \left(\sum_{i=1}^{3}\sum_{j=1}^{3} s_{ij}\, s_{ij}\right)^{1/2}, \quad \dot{\varepsilon}^{\text{c}} = \left(\frac{2}{3}\right)^{1/2} \left(\sum_{i=1}^{3}\sum_{j=1}^{3} \dot{\varepsilon}^{\text{c}}_{ij}\, \dot{\varepsilon}^{\text{c}}_{ij}\right)^{1/2}, \tag{10}$$

where s_{ij} are the deviatoric stress components, the computational model assumes that the multidimensional material creep behaviour still obeys the power-law function given in equation (1 *a*). Therefore the extended tensor formulation of equation (1 *a*) is now simply given as

$$\dot{\varepsilon}^{\text{c}} = B\sigma^n, \tag{11}$$

where

$$B = A_1 \left(\frac{1}{E}\right)^n \left(\frac{b}{d}\right)^q \exp\left(-\frac{Q_{\text{c}}}{RT}\right) \approx A_1 \left(\frac{1}{E}\right)^n \exp\left(-\frac{Q_{\text{c}}}{RT}\right).$$

The plastic creep deformation is considered to be incompressible, that is $\dot{\varepsilon}^{c}_{11}+\dot{\varepsilon}^{c}_{22}+\dot{\varepsilon}^{c}_{33}=0$, and the elasticity is considered isotropic.

Axisymmetric finite-element models were constructed to simulate the indentation response of elasto-plastic solids. Figure 1 (*b*) schematically shows the conical indenter, where $\theta=68^{\circ}$ is the included half-angle of the conical indenter. Figure 1 (*c*) shows the mesh design for axisymmetric finite-element calculations. The semi-infinite substrate of the indented solid was modeled using 12 000 four-noded bilinear axisymmetric quadrilateral elements, where a fine mesh near the contact region and a gradually coarser mesh further from the contact region were designed to ensure numerical accuracy. Finite deformation and, consequently, pile-up or sink-in effect during indentation creep were rigorously accounted for in the computations. More details of the computational model set-up can be found elsewhere (Dao *et al*. 2001).

The load was linearly increased from 0 to the maximum value within a short period of 0.1 s and kept constant afterwards. When the maximum load was reached at $t=0.1$ s, the minimum number of contact elements in the contact zone was no fewer than seven in each finite-element method (FEM) computation. The mesh was well tested for convergence and was determined to be insensitive to far-field boundary conditions. A commercial general-purpose finite-element package ABAQUS (ABAQUS Inc. 2002) was used. A user subroutine was constructed in order to integrate the power-law creep material behaviour.

§ 3. Results

3.1. *Self-similar indentation creep under a constant load*

Figure 2 (solid curves) shows the experimentally measured displacement u, the indenter velocity $\dot{u}$ and the average equivalent stress $\overline{\sigma}$ of the Al–5.3 mol% Mg solid-solution alloy as functions of time; the load is $F=0.39$ N and the test temperature $T=773$ K. It is clear from figure 2 that the stress is a decreasing function of indentation time, and consequently the indenter velocity also decreases monotonically with time. The ratio $\dot{u}/u$, that is the indentation strain rate, is again a decreasing function of indentation time. An indentation creep test corresponds to a stress dip test that can be continuously performed during a conventional uniaxial creep test. The dashed curves in figure 2 show the corresponding computational results, calculated with Young's modulus $E=37.8$ GPa, Poisson's ratio $\nu=0.33$, stress exponent $n=3.2$ and the creep constant $B=7.76\times10^{-7}\,\mathrm{MPa}^{-3.2}\,\mathrm{s}^{-1}$ in equation (11). The computational results of u, $\dot{u}$ and $\overline{\sigma}$ are essentially overlapping with their corresponding experimental curves. The excellent agreement between computational results and the experiments indicates that the rate-dependent power law of equation (11) describes the indented material's constitutive behaviour fairly well. It is worth noting that the elastic deformation in equations (9)–(11) also needs to be accurately taken into account in order to obtain such a good match as shown in figure 2.

One of the central assumptions in deriving the constitutive relation (1 *b*) is that the indentation creep under a constant-load is self-similar. Figure 3 shows the calculated maximum principal strain developed during the indentation creep at $t=0.1$, 10, 40, 200 and 1200 s. It is evident that the strain distribution patterns are self-similar starting from $t=10$ s, although some very minor differences can be found in details at $t=10$ s. At $t=0.1$ s, where the maximum load was just achieved,

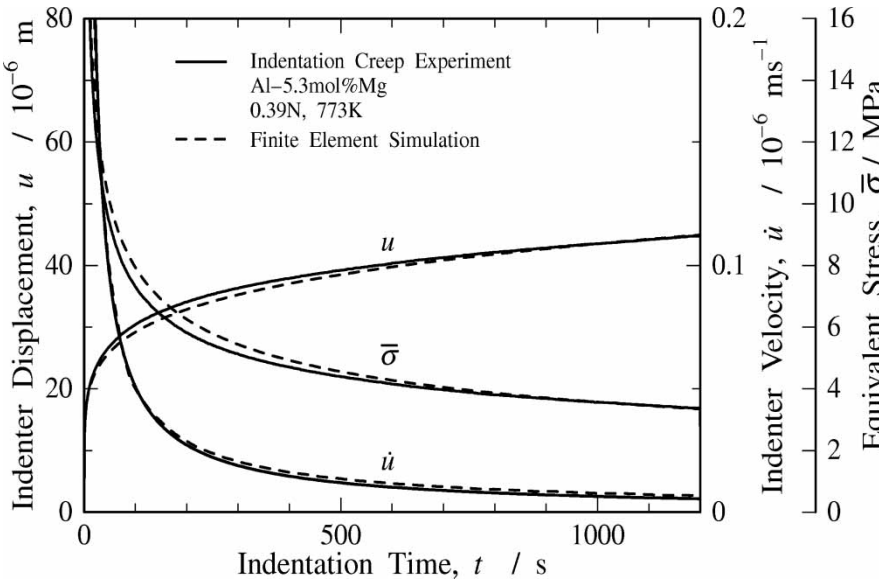

Figure 2. Experimentally measured (—) as well as the corresponding computationally obtained (- - -) results of the displacement u, the indenter velocity $\dot{u}$ and the average equivalent stress $\bar{\sigma}$ of the Al–5.3 mol% Mg solid-solution alloy as functions of time (load $F = 0.39$ N; test temperature $T = 773$ K).

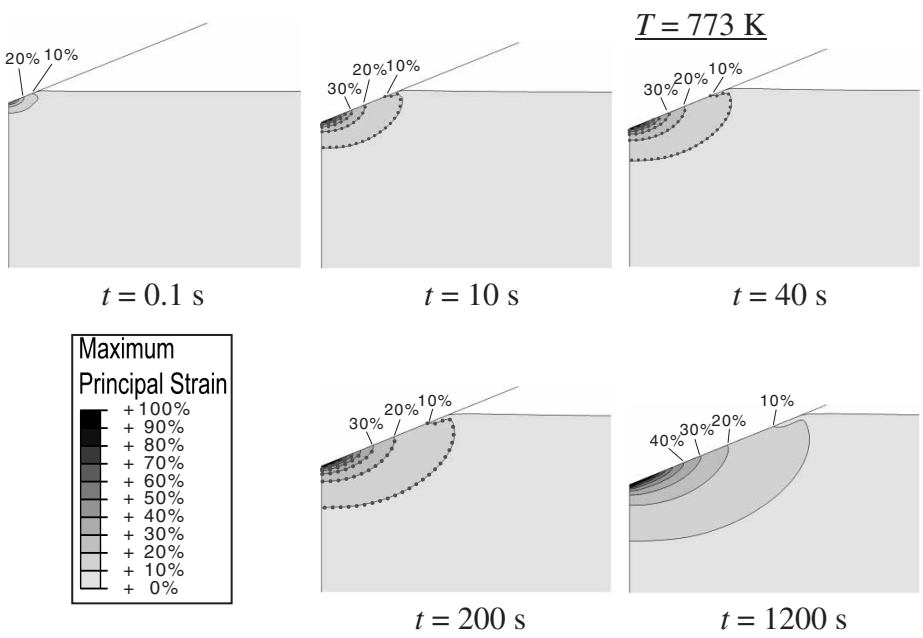

Figure 3. Calculated maximum principal strain contours for $T = 773$ K during indentation creep at $t = 0.1$, 10, 40, 200 and 1200 s. The dotted contour lines are the corresponding contour lines at $t = 1200$ s, proportionally rescaled and overlaid on top of the constant-strain contour lines at $t = 10$, 40 and 200 s. The strain distribution patterns are self-similar starting at $t = 10$ s.

the strain distribution is roughly similar, but not exactly self-similar, to that observed in later stages after the initial transient period.

Additional indentation creep experiments were conducted at different test temperatures. Figure 4 shows indentation creep curves of Al–5.3 mol% Mg solid-solution alloy at six different temperatures from 573 K to 773 K ($0.63T_m$ to $0.85T_m$). When a diamond conical indenter is pressed into the hot material, the indenter displacement rapidly increases within a short time and then slowly penetrates the material by creeping. The indentation displacement u (and the indentation velocity $\dot{u}$) increases with increasing test temperature at the same indentation time t. The indenter displacement also increases with the passage of indentation time, and it would finally reach a stationary value. The indenter displacement for 1200 s at 773 K is about three times that at 573 K, and the final stationary value clearly increases with rising test temperature. From these curves, we can extract and evaluate the indented material's creep constitutive parameters.

3.2. *Power-law creep exponent and its transition*

In figure 5, the indenter velocities are plotted against the corresponding indenter displacements, both on logarithmic scales. The experimental data lie on a family of parallel straight lines at each test temperature, except for the initial transient stage right after loading and the range beyond the measurement limit of a LVDT. It should be noted that the constitutive equation of indentation creep, equation (1 *b*), holds phenomenologically when the experimental plots fall on the straight line. From analogous reasoning to equation (7), the indentation creep on the straight-line region can be interpreted to be in a steady state. Equation (2) indicates that the slope of the straight lines corresponds to $1 - 2n$. The n values so obtained are constant at about 3.2 at all test temperatures. On the other hand, applying either equation (2) or equation (8) to analyse the computational indentation creep curves shown in figure 2, one can accurately obtain the originally introduced creep exponent of the indented material, that is $n = 3.2$; similarly, accurate n-value extractions were also achieved using different creep exponents n in the computations.

Figure 6 (*a*) shows the experimentally measured indentation strain rate versus normalized average equivalent stress at 573 and 590 K, both on logarithmic scales. From equation (8), the two slopes of the straight lines allow us to determine the stress exponents. The stress exponent n changes distinctively from 4.8 to 3.2 at a critical stress level $\overline{\sigma}_c$, as indentation creep proceeds; the indentation creep for $n = 4.8$ takes place in the stress range H† when $\overline{\sigma} > \overline{\sigma}_c$, and that of $n = 3.2$ occurs in the stress range M† when $\overline{\sigma} < \overline{\sigma}_c$. The critical stresses $\overline{\sigma}_c$ were estimated experimentally to be 72.5 MPa and 52.5 MPa at temperatures of 573 K and 590 K respectively. It is very likely that the measured $\overline{\sigma}_c$-value in the indentation creep test corresponds to a critical transition stress in the indented material's creep behaviour. To confirm this and to check whether the self-similarity assumption is still preserved when there is a sudden n-value jump, computational runs were performed assuming a change in creep exponent n from 5.0 to 3.0 at a critical stress σ_c in equation (1 *a*) or equation (11). The input parameters used and the results obtained are listed in table 2 and shown in figures 6 (*b*) and 7.

†For convenience, the medium-stress range of $n \approx 3$ is often denoted by the symbol M, and the low- and high-stress ranges of $n \approx 5$ are represented by the symbols of L and H, respectively.

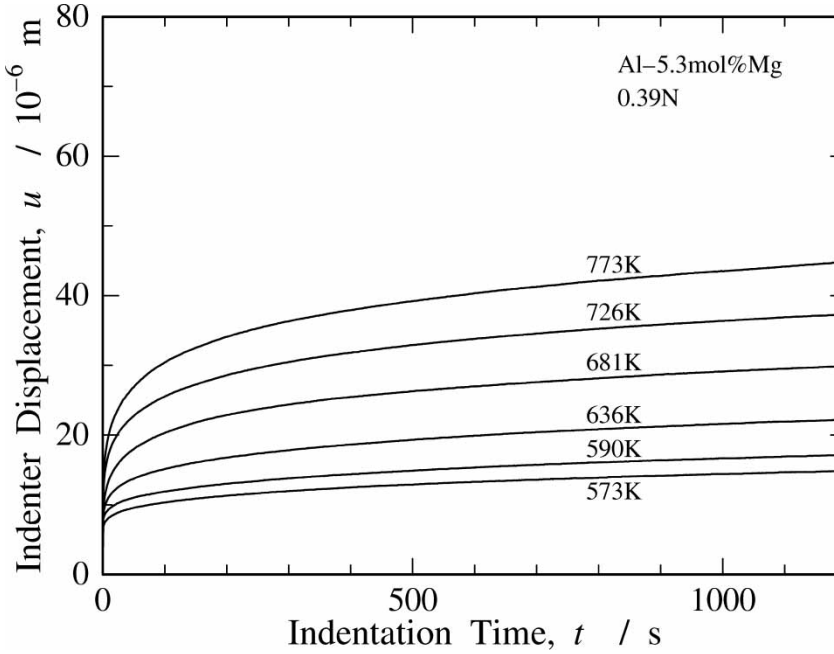

Figure 4. Indentation creep curves of Al–5.3 mol% Mg solid-solution alloy with a constant load of 0.39 N measured at $T = 573$, 590, 636, 681, 726 and 773 K.

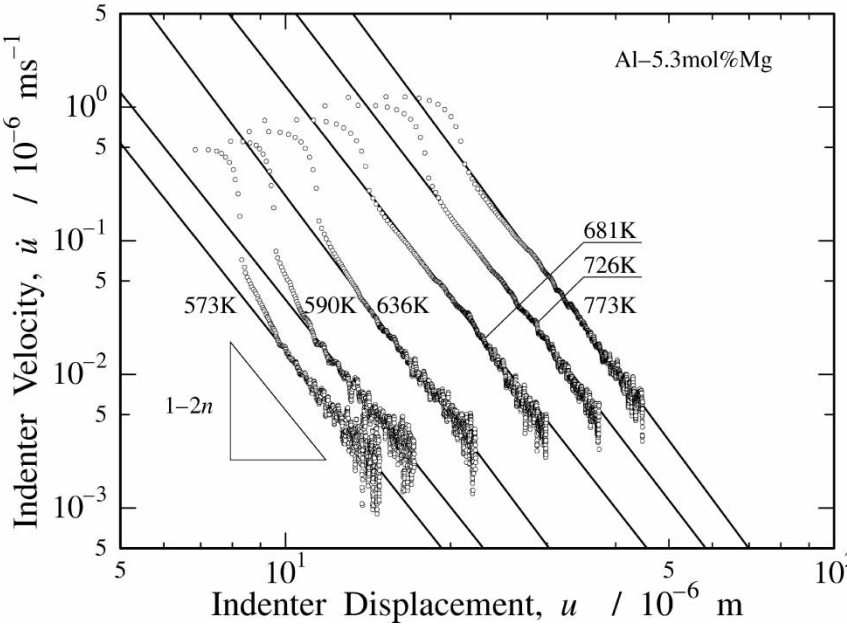

Figure 5. Logarithmic plots of indenter displacement u versus indenter velocity $\dot{u}$ of Al–5.3 mol% Mg solid-solution alloy. The experimental data lie on a family of parallel straight lines at each test temperature, except for the initial transient stage right after loading and the range beyond the measurement limit of the LVDT.

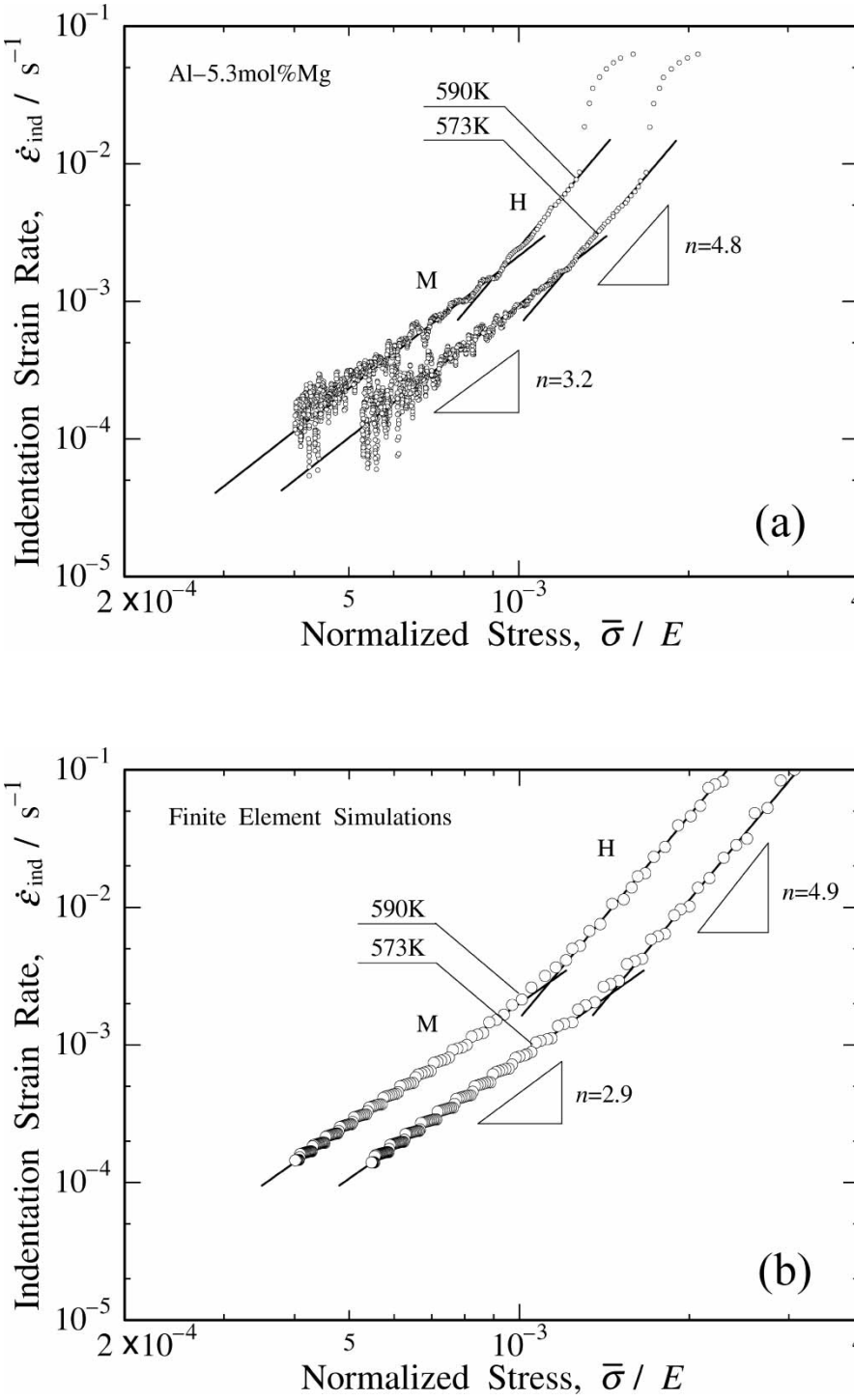

Figure 6. (*a*) Experimentally measured indentation strain rate versus normalized average equivalent stress at 573 and 590 K, both on logarithmic scales. The n value changes distinctively from 4.8 to 3.2 at a critical stress level $\bar{\sigma}_c$. (*b*) Corresponding computational results of indentation strain rate versus normalized average equivalent stress.

Table 2. FEM simulations of the creep exponent change. Input parameters and results are tabulated.

Input parameters								FEM results			
			$\overline{\sigma} > \overline{\sigma}_c$		$\overline{\sigma} < \overline{\sigma}_c$			$\overline{\sigma}_c$ (MPa) (pile-up considered)	$\overline{\sigma}_c$ (MPa) (pile-up not considered)	n	
T (K)	E (GPa)	ν	n	B ($MPa^{-5}\,s^{-1}$)	n	B ($MPa^{-3}\,s^{-1}$)	σ_c (MPa)			$\overline{\sigma} > \overline{\sigma}_c$	$\overline{\sigma} < \overline{\sigma}_c$
573	58.0	0.33	5.0	2.25×10^{-13}	3.0	1.18×10^{-9}	72.5	69.3	77.7	4.9	2.9
590	57.1	0.33	5.0	1.13×10^{-12}	3.0	3.11×10^{-9}	52.5	51.9	60.8	4.9	2.9

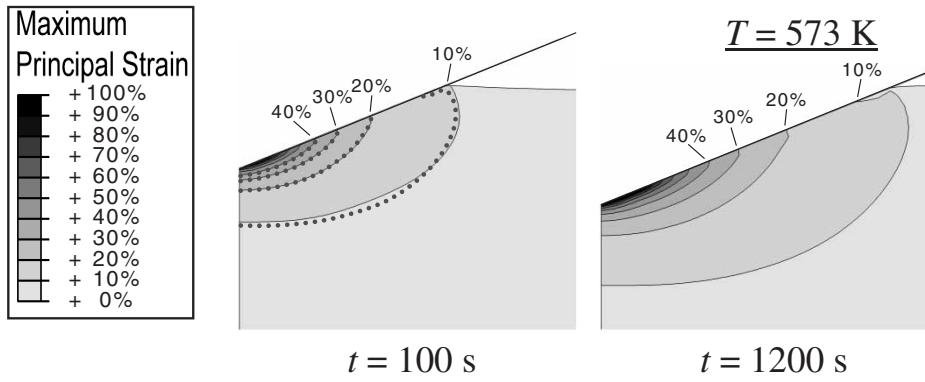

Figure 7. Calculated maximum principal strain contours for $T = 573$ K during indentation creep at $t = 100$ and 1200 s. The dotted contour lines are the corresponding contour lines at $t = 1200$ s, proportionally rescaled and overlaid on top of the constant strain contour lines at $t = 100$ s. The strain contours at $t = 100$ s and $t = 1200$ s are roughly self-similar; they only differ in certain minor details.

A commonly observed phenomenon of indentation experiments is that the material around the indentation impression tends to deform upwards (pile-up) or downwards (sink-in) with respect to the original surface. Note that pile-up or sink-in behaviour is closely related to both the plastic and the elastic properties during indentation creep experiments. To account for the pile-up or sink-in phenomenon, nonlinear large strains, finite rigid-body displacements and finite rigid-body rotations in addition to both the plastic strain-rate hardening and the elasticity are all carefully considered in the computational model. For the typical parameters used in the current study, pile-up was found in all cases, as observed in figure 7. When the pile-up effect is carefully taken into account by the FEM simulations, it is evident that the $\overline{\sigma}_c$ value extracted from an indentation creep curve corresponds closely to, and is a good estimation of, the indented material's σ_c value. Figure 7 shows the computed maximum principal strain contours at $T = 573$K. At $t = 100$ s, the indentation is still in the high-stress range of $n \approx 5$ and, at $t = 1200$ s, the indentation is well within the steady-state range of $n \approx 3$. The strain contours at $t = 100$ s and $t = 1200$ s are roughly self-similar; they only differ in certain minor details. Comparing figure 7 with figure 3, the strain distribution patterns at $t = 1200$ s are very much similar, showing again that the earlier transient behaviour near the transition stress $\overline{\sigma}_c$ are diminishing with longer indentation times.

3.3. *Activation energy for indentation creep*

Figure 8 shows the Arrhenius plot of K values obtained from analysing the data lying on the parallel straight lines in figure 5. As mentioned earlier, the K parameter, given by $K = \dot{\varepsilon}_{\mathrm{ind}}(Eu^2/F)^n$, represents an indentation strain rate in which the stress dependence is compensated, so that the K value is uniquely determined at a given temperature and the dependence of K value upon temperature can be expressed by a straight line in the Arrhenius plot diagram. According to equation (4), the slope of the straight line corresponds to $-Q_{\mathrm{c}}/2.3RT_{\mathrm{m}}$. The activation energy for creep so obtained is $Q_{\mathrm{c}} = 123\,\mathrm{kJ\,mol^{-1}}$, which agrees well with the value of $130\,\mathrm{kJ\,mol^{-1}}$ obtained for the mutual diffusion of an Al–Mg solid-solution alloy (Brandes *et al.* 1998). It follows that the indentation strain rate in the range M of $n = 3.2$ is proportional to a diffusion coefficient of the solid-solution alloy. The finding suggests that the indentation creep is rate controlled by the viscous glide of dislocations, which depends on dragging resistance that arises from the interaction of solute atmosphere with gliding dislocations.

3.4. *Back stress acting on moving dislocations*

Taking into account the back stress σ_{b} acting on moving dislocations (Cadek 1988), equation (7) can be rewritten as

$$\dot{\varepsilon}_{\mathrm{ind}} = A_4\left(\frac{\overline{\sigma} - \sigma_{\mathrm{b}}}{E}\right)^n \left(\frac{b}{d}\right)^q \exp\left(-\frac{Q_{\mathrm{c}}}{RT}\right), \tag{12}$$

where A_4 is a constant. When the back stress is the athermal resistance due to long-range interaction of other dislocations, the resistance is often called an internal

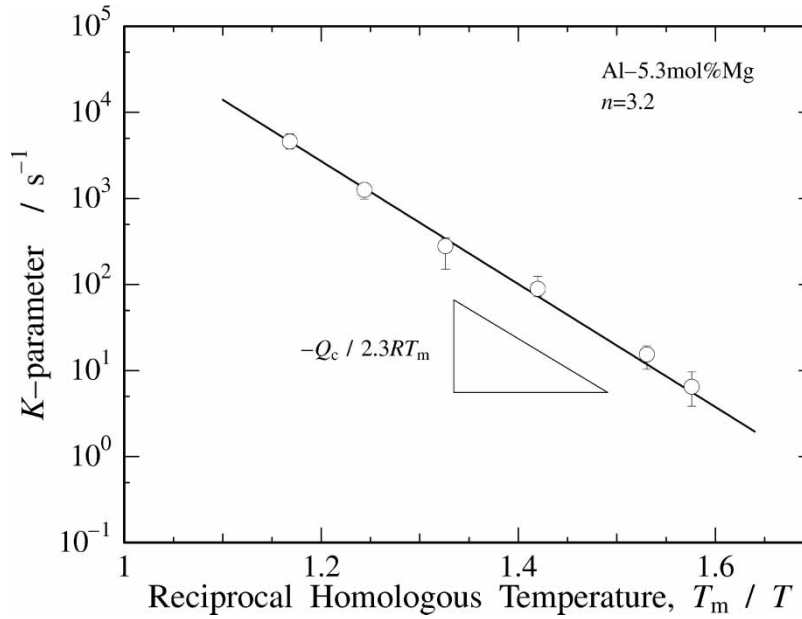

Figure 8. Arrhenius plot of the K parameter, $K = \dot{\varepsilon}_{\mathrm{ind}}(Eu^2/F)^n$.

stress σ_i, which is generally expressed by (Taylor 1938, Carrington *et al.* 1960, Yoshinaga *et al.* 1985)

$$\sigma_i = \alpha\mu b M \rho^{1/2}, \tag{13}$$

where α is a constant depending on dislocation arrangement, μ is the shear modulus, M is the Taylor factor ($M \approx 3.06$ for fcc polycrystals (Taylor 1938)) and ρ is the density of free dislocations. For the region of $n \approx 3$ in an Al–Mg solid-solution alloy, it is known that dislocations are distributed homogeneously without forming cell structures at high temperatures (Horiuchi and Otsuka 1972, Vagarali and Langdon 1982) and the free-dislocation density during steady-state creep depends on the applied stress as

$$\rho \propto \frac{1}{b^2}\left(\frac{\overline{\sigma}}{\mu}\right)^m, \tag{14}$$

where m is a constant of about 2. Connecting equation (14) to equation (13), the internal stress is approximately proportional to the applied stress, so that equation (12) can be expressed as the same $\dot{\varepsilon}_{ind}^{1/n} \propto \overline{\sigma}/E$ dependence as in equation (7) at a given temperature. If the relation $\dot{\varepsilon}_{ind}^{1/n} \propto \overline{\sigma}/E$ describes the data completely, the experimental curves should be a family of straight lines passing though the origin of the coordinate axes, which is indeed the case as shown in figure 9. These curves are plotted with the data that lie on the straight lines with $n = 3.2$ in figure 5. When the data points at each test temperature in figure 9 are linearly extrapolated, the corresponding extrapolation lines all pass through the origin of the coordinate axes. The finding suggests that the back stress in the range M ($n = 3.2$) is the internal stress, which is connected to long-range interaction of dislocations.

3.5. *Comparison with results obtained from conventional uniaxial creep tests*

Conventional uniaxial creep test results (Pahutova and Cadek 1979, Sato and Oikawa 1988) on Al–Mg solid-solution alloy showed that the stress exponent at a

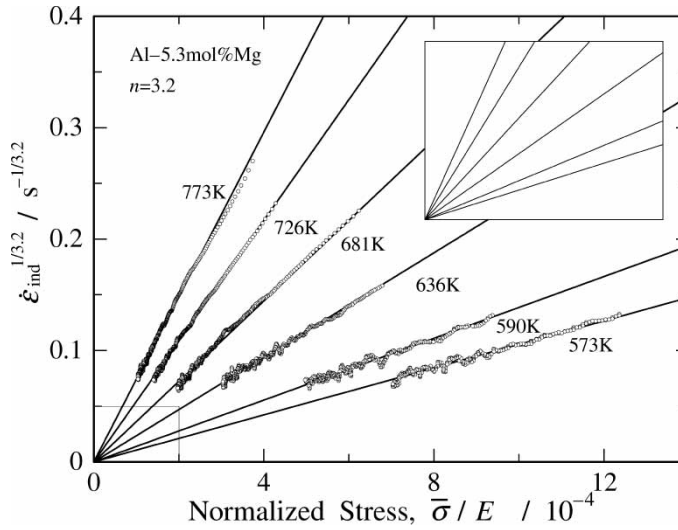

Figure 9. Relationship of $\dot{\varepsilon}_{ind}^{1/n}$ versus $\overline{\sigma}/E$. When the data points at each test temperature in the figure are linearly extrapolated, the corresponding extrapolation lines all pass through the origin of the coordinate axes.

Table 3. Comparison of indentation creep test results and conventional creep test results in the range M ($n \approx 3$).

Creep test method	Test materials	T (K)	Stress range $\bar{\sigma}$ (MPa)	n	Activation energy for creep (kJ mol^{-1})
Indentation (current study)	Al–5.3 mol% Mg alloy	573–773	3.6–72.5	3.2	123
Tension (Horiuchi and Otsuka 1972)	Al–5.1 mol% Mg alloy	601–734	2.0–68.6	2.8–3.0	135–144
Tension (Kucharov *et al.* 1974, Pahutova and Cadek 1979)	Al–5.5 mol% Mg alloy	623	6.7–70.0	3.2	139–141

given temperature typically takes a constant either of 3 or 5 depending on the applied stress. For convenience, the medium-stress range of $n \approx 3$ is denoted by M, and the low- and high-stress ranges of $n \approx 5$ are represented by L and H respectively. This kind of deformation characteristics can be explained by considering changes in the interaction between moving dislocations and the solute atmosphere. At high temperatures and low stresses where the diffusion rate of solute atoms is sufficiently high in comparison with dislocation velocity, the dragging resistance falls off with rising temperature or decreasing stress. In the range L, the solute atoms can completely follow moving dislocations by diffusional migration, so that the presence of solute atmosphere exhibits little influence on the dislocations in motion. In the range H, the dislocation velocity is considerably higher than the diffusion rate of solute atoms, so that mobile dislocations can break away from their solute atmosphere at a critical stress level or higher. Experimental results (Cadek 1988) showed that creep in the ranges L and H is rate controlled by a recovery process that depends on climb motion of dislocations, similar to creep deformation of pure metals with $n \approx 5$. In contrast, creep in the range M is rate controlled by the glide motion of dislocations which drag the solute atmosphere, and the activation energy for creep is almost equal to that for mutual diffusion of solid-solution alloy.

Table 3 lists the results of our indentation creep test and tensile creep tests found in the literature (Horiuchi and Otsuka 1972, Kucharov *et al.* 1974, Pahutova and Cadek 1979) within the $n \approx 3$ region. Under similar conditions, the two testing methods give almost the same stress exponents and activation energies for creep. These results demonstrate that indentation creep test results are equivalent to conventional uniaxial creep test results in the dislocation creep regime.

§4. Discussion

At $T = 573$ and 590 K, the n transition from 4.8 to 3.2 shows that the creep rate-controlling process changes from the climb motion to the glide motion of dislocations at a certain stress level as indentation creep proceeds. Solid-solution alloys at high temperatures may deform plastically by five different deformation mechanisms, so that the predominant, and thus rate-controlling, mechanism depends decisively on the precise conditions of applied stress, temperature and

microstructure. The possible deformation mechanisms include dislocation climb rate-controlling creep (mechanism 1), dislocation glide rate-controlling creep (mechanism 2), Harper–Dorn creep (mechanism 3), Nabarro–Herring creep (mechanism 4) and Coble creep (mechanism 5). The two mechanisms 1 and 2 interact in a sequential manner, but the other mechanisms 3, 4 and 5 operate independently of each other. Therefore, with all these mechanisms operating, the measured indentation strain rate $\dot{\varepsilon}_{\mathrm{ind}}$ can be expressed as

$$\dot{\varepsilon}_{\mathrm{ind}} = \frac{\dot{\varepsilon}_1 \dot{\varepsilon}_2}{\dot{\varepsilon}_1 + \dot{\varepsilon}_2} + \dot{\varepsilon}_3 + \dot{\varepsilon}_4 + \dot{\varepsilon}_5, \tag{15}$$

where $\dot{\varepsilon}_i$ is the creep rate for the ith deformation mechanism. Under the experimental conditions of $\overline{\sigma}/E = 10^{-4} - 10^{-3}$, $d/b \approx 10^6$ and $T/T_{\mathrm{m}} = 0.63$–0.85, the values of $\dot{\varepsilon}_3$, $\dot{\varepsilon}_4$ and $\dot{\varepsilon}_5$ are negligibly small (Mohamed and Langdon 1975). Thus, equation (15) can be reduced to

$$\dot{\varepsilon}_{\mathrm{ind}} = \frac{\dot{\varepsilon}_1 \dot{\varepsilon}_2}{\dot{\varepsilon}_1 + \dot{\varepsilon}_2}. \tag{16}$$

When an applied stress is greater than the critical stress $\overline{\sigma}_{\mathrm{c}}$ necessary for breakaway of dislocations from their solute atmosphere, it is anticipated that the solute atmosphere no longer hinders the motion of dislocations. When $\dot{\varepsilon}_1 \ll \dot{\varepsilon}_2$ under high applied stresses $\overline{\sigma} > \overline{\sigma}_{\mathrm{c}}$, we have $\dot{\varepsilon}_{\mathrm{ind}} \approx \dot{\varepsilon}_1$. This means that creep in the high-stress regime is rate controlled by some recovery process dependent on the climb motion of dislocations. In this case, it is known that the steady-state creep rate is typically proportional to the fifth power of applied stress, that is $\dot{\varepsilon}_{\mathrm{ind}} \propto (\overline{\sigma}/E)^5$. On the other hand, when the glide velocity of dislocations is of the order of the climb velocity due to atmosphere drag, it follows that $\dot{\varepsilon}_{\mathrm{ind}} \approx \dot{\varepsilon}_2$. Accordingly, the creep in low-stress range where $\overline{\sigma} < \overline{\sigma}_{\mathrm{c}}$ is rate controlled by viscous glide of dislocations, and $\dot{\varepsilon}_{\mathrm{ind}} \propto (\overline{\sigma}/E)^3$ is typical (Poirier 1985).

According to Friedel (1964), the critical stress for breakaway of dislocations from their solute atmosphere is inversely proportional to temperature. Similarly, the experimental result indicates that the critical stress level for the n-value transition significantly decreases as temperature increases; the values of $\overline{\sigma}_{\mathrm{c}}/E$ for 573 K and 590 K are 1.24×10^{-3} and 9.19×10^{-4} respectively.

For the case of $T = 773$ K in figure 5, the average equivalent stress $\overline{\sigma}$ decreases from 13.5 to 3.6 MPa as indentation steady-state creep proceeds. If the critical stress $\overline{\sigma}_{\mathrm{c}}$ at 773 K is higher than 13.5 MPa, one cannot detect the existence of the stress range H ($n = 4.8$) through the instrumented microindentation technique. In fact, the stress range of $n = 4.8$ disappears when $T \geqslant 636$ K and only the stress range of $n = 3.2$ can be detected during indentation creep tests.

§ 5. Conclusions

Instrumented indentation is a convenient technique that enables us to explore the mechanical properties of small-volume materials at high temperatures. We have performed indentation creep tests, where a self-similar indenter is pressed into a depth of 100 μm or less from the material surface. The current experimental setup for indentation creep test has a number of advantages.

(i) Specimens can be small in size and simple in shape.
(ii) Mechanical properties can be explored for a selected local region.

(iii) The testing time required is relatively short.
(iv) Response to a load application mechanism is satisfactory.
(v) High-temperature and high-stress conditions can be easily realized.
(vi) A vacuum or inert-gas test atmosphere can be prepared without difficulty.

Carefully designed indentation creep experiments together with corresponding finite-element computations were carried out in order to establish a robust and systematic method to extract creep properties accurately during indentation creep tests. It was confirmed that indentation creep tests of Al–5.3 mol% Mg solid-solution alloy at temperatures ranging from 573 to 773 K can be effectively used to extract material parameters equivalent to those obtained from conventional uniaxial creep tests in the dislocation creep regime. The key results of this study can be summarized as follows.

(1) If the indented material is a power-law creep material (i.e. obeys equation (11)), the indentation creep strain field is self-similar during a constant-load creep test, except during a short transient period on initial loading or when there is a deformation mechanism change.
(2) When the temperature and grain size are kept constant, the creep exponent n can be robustly extracted using

$$n = \frac{\partial(\ln \dot{\varepsilon}_{\mathrm{ind}})}{\partial \ln(\overline{\sigma}/E)}$$

or

$$n = \frac{1}{2}\left(1 - \frac{\partial(\ln \dot{u})}{\partial(\ln u)}\right).$$

(3) For the Al–5.3 mol% Mg solid-solution alloy used in this study, the creep stress exponent n varies distinctively from 4.8 to 3.2 at a critical stress level as indentation creep proceeds. This n-value transition indicates that the creep rate-controlling process changes from dislocation climb to viscous glide at a critical stress, which decreases significantly with increasing temperature.
(4) In the stress range where $\sigma < \sigma_c$ ($n = 3.2$), the back stress acting on moving dislocations is proportional to the average equivalent stress (applied stress) occurring in the region just below the impression. This finding suggests that the back stress is the internal stress related to long-range interaction with dislocations.
(5) The activation energy Q_c for creep was found to be 123 kJ mol^{-1}, which is close to the activation energy for mutual diffusion of this alloy, 130 kJ mol^{-1}.
(6) Experimental results indicate that the creep of the solid-solution alloy under the condition of $n = 3.2$ and $Q_c = 123$ kJ mol^{-1} is rate controlled by viscous glide of dislocations that drag solute atmosphere. These results are in good agreement with those obtained from conventional uniaxial creep tests in the dislocation creep regime.

Acknowledgements

The authors gratefully acknowledge insightful suggestions from Professor Subra Suresh during the course of this study. M.F. acknowledges the support by Overseas

Researcher Fund of Nihon University. M.D. acknowledges the support by the Defense University Research Initiative on Nano Technology which is funded at the Massachusetts Institute of Technology by the Office of Naval Research under grant N00014-01-1-0808.

References

ABAQUS Inc., 2002, ABAQUS, Version 6.3 (Pawtucket, Rhode Island: ABAQUS Inc.)
Asif, S. A. S., and Pethica, J. B., 1997, *Phil. Mag.* A, **76**, 1105.
Atkins, A. G., Silverio, A., and Tabor, D., 1966, *J. Inst. Metals*, **94**, 369.
Bolshakov, A., and Pharr, G. M., 1998, *J. Mater. Res.*, **13**, 1049.
Brandes, E. A., Brook, G. B., and Smithells, C. J., 1998, *Smithells Metals Reference Book*, Seventh edition, edited by E. A. Brandes and G. B. Brook (Oxford: Butterworth–Heinemann).
Cadek, J., 1988, *Creep in Metallic Materials* (Amsterdam: Elsevier).
Carrington, W., Hale, K. F., and McLean, D., 1960, *Proc. R. Soc.* A, **259**, 203.
Cheng, Y. T., and Cheng, C. M., 2001, *Phil. Mag. Lett.*, **81**, 9.
Dao, M., Chollacoop, N., Van Vliet, K. J., Venkatesh, T. A., and Suresh, S., 2001, *Acta mater.*, **49**, 3899.
Field, J. S., and Swain, M. V., 1995, *J. Mater. Res.*, **10**, 101.
Friedel, J., 1964, *Dislocations* (Oxford: Pergamon).
Fujiwara, M., and Otsuka, M., 1999, *J. Japan. Inst. Metals*, **63**, 760; 2001, *Mater. Sci. Engng*, **A319**, 929.
Gerberich, W. W., Nelson, J. C., Lilleodden, E. T., Anderson, P., and Wyrobek, J. T., 1996, *Acta mater.*, **44**, 3585.
Hill, R., 1983, *The Mathematical Theory of Plasticity* (Oxford: Clarendon).
Horiuchi, R., and Otsuka, M., 1972, *Trans. Japan Inst. Metals*, **13**, 283.
Johnson, K. L., 1970, *J. Mech. Phys. Solids*, **18**, 115.
Kucharov, K., Saxl, I., and Cadek, J., 1974, *Acta metall.*, **22**, 465.
Li, J. C. M., 2002, *Mater. Sci. Engng*, **A322**, 23.
Li, W. B., Henshall, J. L., Hooper, R. M., and Easterling, K. E., 1991, *Acta metall.*, **39**, 3099.
Lucas, B. N., and Oliver, W. C., 1999, *Metall. Mater. Trans.* A, **30**, 601.
Mackerle, J., 2001, *Finite Element Anal. Des.*, **37**, 811.
Mayo, M. J., and Nix, W. D., 1988, *Acta metall.*, **36**, 2183.
Mohamed, F. A., and Langdon, T. G., 1975, *Scripta metall.*, **9**, 137.
Mukherjee, A. K., Bird, J. E., and Dorn, J. E., 1969, *Trans. Am. Soc. Metals*, **62**, 155.
Mulhearn, T. O., and Tabor, D., 1960, *J. Inst. Metals*, **89**, 7.
Oliver, W. C., and Pharr, G. M., 1992, *J. Mater. Res.*, **7**, 1564.
Pahutova, M., and Cadek, J., 1979, *Phys. Stat. sol.* (a), **56**, 305.
Poirier, J. P., 1985, *Creep of Crystals: High-temperature Deformation Processes in Metals, Ceramics, and Minerals* (Cambridge University Press).
Prakash, O., 1996, *The Johannes Weertman symposium*, edited by R. J. Arsenault, D. Cole, T. Gross, G. Kostorz, P. K. Liaw, S. Parameswaran and H. Sizek (Anaheim, California: Minerals, Metals & Materials Society).
Sargent, P. M., and Ashby, M. F., 1992, *Mater. Sci. Technol.*, **8**, 594.
Sato, H., and Oikawa, H., 1988, *Scripta metall.*, **22**, 87.
Tabor, D., 1951, *The Hardness of Metals* (Oxford: Clarendon).
Taylor, G. I., 1938, *J. Inst. Metals*, **62**, 307.
Vagarali, S. S., and Langdon, T. G., 1982, *Acta metall.*, **30**, 1157.
Yoshinaga, H., Matsuo, S., and Kurishita, H., 1985, *Trans. Japan Inst. Metals*, **26**, 423.